2011

# Structure and magnetism of MnAu nanoclusters

X. Wei
*University of Nebraska-Lincoln*

Damien Le Roy
*University of Nebraska-Lincoln*, damien.le-roy@grenoble.cnrs.fr

Ralph Skomski
*University of Nebraska - Lincoln*, rskomski@unl.edu

Xingzhong Li
*University of Nebraska - Lincoln*, xzli@unl.edu

Zhiguang Sun
*University of Nebraska - Lincoln*, zsun3@unl.edu

*See next page for additional authors*

# Structure and magnetism of MnAu nanoclusters

X. Wei,[1,3,a)] D. Le Roy,[1,3] R. Skomski,[1,3] X. Z. Li,[3] Z. Sun,[3] J. E. Shield,[2,3] M. J. Kramer,[4] and D. J. Sellmyer[1,3]
[1]*Department of Physics and Astronomy, University of Nebraska, Lincoln, Nebraska 68588, USA*
[2]*Department of Mechanical Engineering, University of Nebraska, Lincoln, Nebraska 68588, USA*
[3]*Nebraska Center for Materials and Nanoscience, University of Nebraska, Lincoln, Nebraska 68588, USA*
[4]*Ames Laboratory, Ames, Iowa 50011, USA*

(Presented 18 November 2010; received 4 October 2010; accepted 30 November 2010; published online 31 March 2011)

Equiatomic MnAu clusters with average sizes of 4 and 10 nm are produced by inert-gas condensation. As-produced clusters are used to form both dense cluster films and films with clusters embedded in a W matrix with a cluster volume fraction of 25%. Both structure and magnetism are size-dependent. Structural analysis of the 10 nm clusters indicate a distorted tetragonal body-centered cubic structure with lattice parameters $a = 0.315$ and $c = 0.329$ nm. The 4 nm clusters have a partially ordered tetragonal $L1_0$ structure with lattice parameters $a = 0.410$ nm and $c = 0.395$ nm. Magnetic properties of the clusters show evidence at low temperatures of mixed ferromagnetic and antiferromagnetic interactions and ordering as well as paramagnetic spins. Saturation moments are as large as 0.54 $\mu_B$ per average Mn atom. The results are compared with earlier theoretical calculations on bulk MnAu. © *2011 American Institute of Physics*.
[doi:10.1063/1.3559502]

## I. INTRODUCTION

Nanoparticles are attracting increased attention due to their unique optical, catalytic, electronic, and magnetic properties.[1–3] For example, unusual crystal and magnetic structures sometimes stabilize in nanoparticles due to their large surface-to-volume ratio and low coordination number on the surface.[4] A particularly interesting class of nanoparticles is alloy nanoparticles for applications in catalysis, which contain noble metals such as Au, Ag, Pt, and transition metals.[5,6] Our focus is on the exploitation of the large atomic magnetic moment of Mn in permanent-magnet and other applications, and theoretical predictions[7] indicate that this may be possible in Mn–Au nanoparticles.

Mn and Au form various compounds, among which $MnAu_4$ is ferromagnetic with a Curie temperature of 373 K,[8] while $MnAu_3$, $MnAu_2$, $Mn_2Au_5$, and MnAu are antiferromagnetic (AFM) with Néel temperatures of 140, 354, 365, and 513 K,[8–11] respectively. Previous first-principle total energy calculations on bulk equiatomic MnAu show that multiple AFM and ferromagnetic (FM) spin structures compete as a function of lattice distortion ratio $c/a$.[12] However, there are no previous experimental investigations on MnAu nanoparticles. A challenge is to use nanostructuring as an approach to create substantial net magnetic moments in structures that are AFM in their bulk equilibrium states. Our focus is on the size-dependence of structure and magnetism of MnAu clusters.

## II. EXPERIMENTAL DETAILS AND STRUCTURAL ANALYSIS

Equiatomic MnAu clusters were deposited from a Mn-50 at. % Au alloy target, via inert-gas condensation in a cluster-deposition system with a base pressure of $10^{-8}$ Torr.[13] The average sizes of the clusters ($d$) were chosen as 4 and 10 nm. Each cluster size was used to produce two types of films, namely, (i) dense cluster films and (ii) clusters embedded in a W matrix. The dense cluster film is a 10 nm thick single cluster layer while the embedded film is fabricated by deposition of alternating cluster layers (0.7 nm in nominal thickness) and W layers (3 nm in thickness), corresponding to a cluster volume fraction of 25%. The size, structure, and morphology of the clusters were examined by transmission electron microscopy (TEM), x-ray diffraction (XRD), and high-resolution electron microscopy (HREM). The composition was examined with energy-dispersive spectroscopy (EDS). A superconductong quantum interference device magnetometer was used to study the magnetism of the clusters, especially the size-dependence of magnetization, coercivity, exchange bias, and vertical magnetization shift.

EDS analysis of the as-produced clusters showed that the Mn content is close to 50 at. %. Figures 1(a) and 1(b) show the TEM images for clusters with average sizes of 4 and 10 nm, respectively. The cluster-size distributions, determined from TEM images, are displayed in 1(c), the rms $\sigma/d$ is 13 and 9% for the 4 and 10 nm clusters, respectively. Figure 1(d) shows a representative HREM image for the 4 nm clusters.

Figure 2 shows the XRD patterns of the as-produced cluster films. For the 10 nm clusters, the diffraction patterns match the tetragonally distorted body-centered-cubic (bcc) type MnAu alloy with the bulk lattice constants $a = 0.315$ nm and $c = 0.329$ nm. For the 4 nm clusters, XRD shows a strong and broad peak at $2\theta \approx 39^{\circ}$. Fast Fourier transforms of HREM images of clusters with $d \leq 5$ nm can be indexed to a slightly tetragonalized fcc structure with $a = 0.410$ nm and $c = 0.395$ nm. As shown by Wang *et al.*,[12] this structure

a)Author to whom correspondence should be addressed. Electronic mail: sunshine@huskers.unl.edu.

 

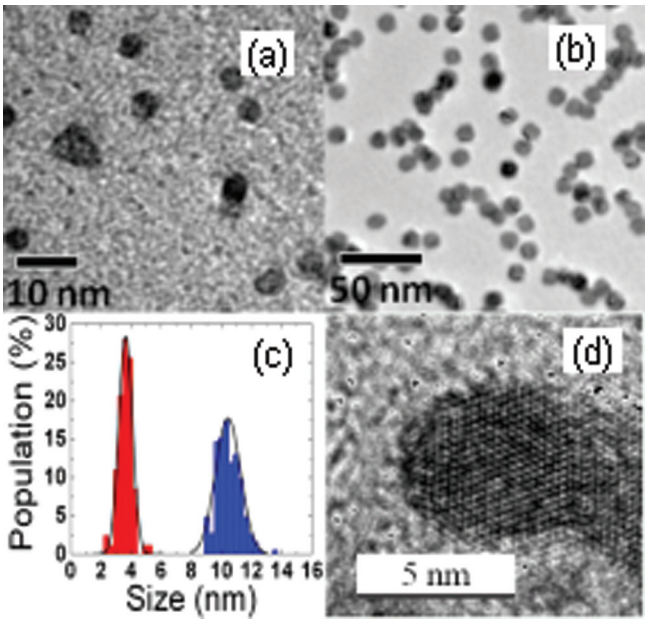


FIG. 1. (Color online) TEM images of as-produced MnAu clusters with average sizes of (a) 4 and (b) 10 nm. Size distributions are shown in (c) and (d) shows the HREM of a 4 nm cluster.

can be considered with a different basis set as a distorted bcc structure. In this way the lattice parameters would be $a = 0.290$ nm and $c = 0.395$ nm. Note that the lattice parameters of the 10 and 4 nm clusters are surprisingly close to previous theoretical predictions[12] of $a = 0.318$ and $c = 0.328$ nm and $a = 0.407$ and $c = 0.392$ nm for the bulk $\beta_2$ and $L1_0$ structures, respectively. The latter structure would produce in XRD an (111) peak at $2\theta = 38.5^{o}$, (200) at $44.5^{o}$, and (002) peak at $46^{o}$, in agreement with the observed pattern.

## III. MAGNETIC PROPERTIES

Figure 3 shows the hysteresis loops taken at 6 K for the embedded (triangles) and dense (circles) cluster films. The inset shows the loop shifts after cooling in a magnetic field of 5 T from 300 to 5 K. The saturation magnetization ($M_s$) is

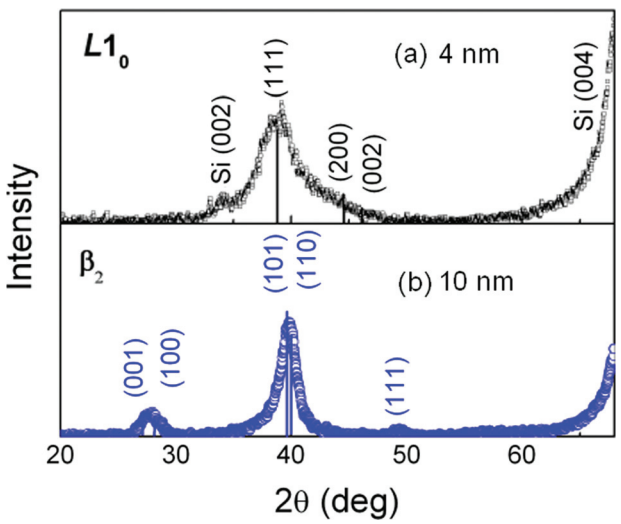


FIG. 2. (Color online) XRD of as-produced MnAu clusters: (a) 4 nm and (b) 10 nm.

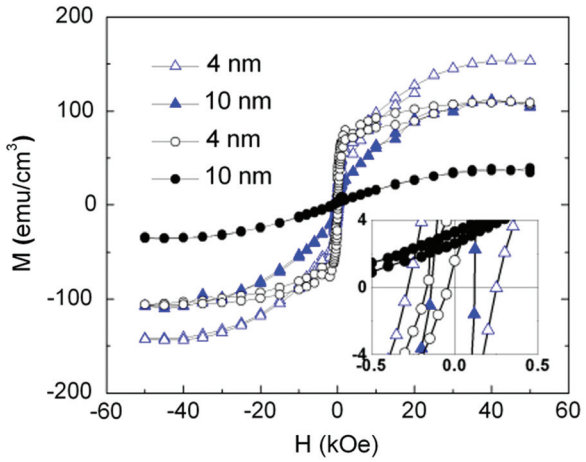


FIG. 3. (Color online) Hysteresis loops taken at 6 K for the embedded (triangle) and dense (circle) cluster films. The 4 and 10 nm clusters are designated by empty and filled symbols, respectively. The inset shows hysteresis loops at low field with loop shifts.

calculated using the cluster volume. The 4 and 10 nm clusters are marked by empty and filled symbols, respectively. As the cluster size decreases from 10 to 4 nm, $M_s$ and coercivity ($H_c$) of the embedded series increase from 110 to 150 emu/cm$^3$ and 70 to 267 Oe, respectively. Exchange bias ($H_{EB}$) and vertical magnetization shift ($\delta m$) are insignificant. Similarly, for the dense series, the magnetization increases from 32 to 110 emu/cm$^3$ while coercivity increases from 70 to 129 Oe. Significant $H_{EB}$ and $\delta m$ are observed. As size decreases, $H_{EB}$ decreases from 116 to 17 Oe while $\delta m$ decreases from 4 to 1% of $M_s$.

Figure 4 shows the zero-field-cooled (ZFC) and field-cooled (FC) $M(T)$ curves for the (a) 4 nm and (b) 10 nm cluster films. The embedded and dense clusters are marked by triangles and circles, respectively. These data show several features. First, there is an apparent strong upturn in the FC data for $T \leq 50$ K, which is most pronounced for 4 nm clusters. This suggests the presence of paramagnetic spin on Mn atoms that are associated with surfaces where the number and strength of exchange interactions are relatively small. Second, there is an apparent ordering or freezing temperature $T_0$, where there are fairly sharp changes in the slope of the FC curves; below $T_0$ there is a significant increase in magnetization that leads to $M_s$ values in Fig. 3 of order 0.54 $\mu_B$/Mn atom (for $M_s = 150$ emu/cm$^3$). The relevant $T_0$ values for the 4 nm particles are about 110 and 50 K for the dense and

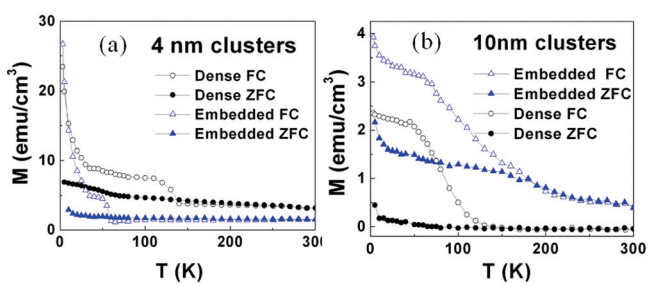


FIG. 4. (Color online) ZFC and FC magnetizations for (a) 4 nm and (b) 10 nm clusters. The embedded and dense cluster films are marked by triangles and circles, respectively.

embedded particles, respectively. For the 10 nm clusters, the $T_0$ values are about 40 and 60 K for the dense and embedded particles, respectively. For the 10 nm particles in particular, the ordering appears to be gradual which may reflect a broader range of exchange interactions.

## IV. DISCUSSION AND CONCLUSION

The magnetic data discussed above are complex in exhibiting features associated with antiferromagnetic and ferromagnetic interactions, as well as paramagnetic spins at low temperatures. The data show features that can be associated with an AFM core with a shell that has spin-glass (mixed) or FM interactions due to enhanced disorder, lattice dilation, or weakened exchange leading to paramagnetic spins at low temperatures. Our dense films show effects of increased intercluster exchange through increased $T_0$ values. The size dependence of our MnAu clusters, that is, the increase of $M_s$ and $H_c$ and the decrease of $H_{EB}$ and $\delta m$ with size reduction can be attributed to a more significant shell and smaller contribution from the core in a core-shell spin structure. It is interesting that the lattice parameters of the 10 and 4 nm MnAu clusters conform to $\beta_2$ and $L1_0$ structures,[12] respectively, for which different AFM spin structures with Mn moments of 3.86 and 3.93 $\mu_B$ are predicted in the bulk.[12] Thus the net moments of the 10 and 4 nm MnAu clusters are probably a result of different AFM cores and their associated uncompensated surface moments. Similar phenomena including exchange bias and magnetization shifts have been reported for various other AFM nanoparticles[14–17]. In these systems also a core-shell spin structure was suggested where the core retains the bulk AFM magnetic structure and the shell with associated defects leads to manifestations of FM or spin-glass interactions.[18–20]

In summary, we have used inert-gas condensation to produce equiatomic MnAu clusters with average sizes of 4 and 10 nm. Structures related to $L1_0$ and $\beta_2$ phases are found for the two sizes. Saturation moments of 0.36 and 0.54 $\mu_B$/Mn atom are obtained for the 10 and 4 nm clusters, respectively. A thorough understanding of the magnetism of these clusters will require additional studies such as neutron diffraction measurements of the spin structure.

## ACKNOWLEDGMENTS

This research is supported by NSF MRSEC (Grant No. DMR 0 820 521), BREM (R.S.), ARPA-E (J.S., D.J.S.), and NCMN.

[1]J. S. Garitaonandia *et al.*, Nano Lett. **8**, 661 (2008).
[2]Y. Liou, M. S. Lee, and K. L. You, Appl. Phys. Lett. **91**, 082505 (2007).
[3]J. L. Lyon, D. A. Fleming, M. B. Stone, P. Schiffer, and M. E. Williams, Nano Lett. **4**, 719 (2004).
[4]J. Penuelas *et al.*, Eur. Phys. J. Spec. Top. **167**, 19 (2009).
[5]Y. Xu and J. Wang, Adv. Mater. **20**, 994 (2008).
[6]Y. Bao, H. Calderon, and K. M. Krishnan, J. Phys. Chem. C **111**, 1941 (2007).
[7]J. Wang, J. Bai, J. Jellinek, and X. Zeng, J. Am. Chem. Soc. **129**, 4110 (2007).
[8]S. Abe, M. Matsumoto, H. Yoshida, S. Mori, T. Kanomata, and T. Kaneko, J. Magn. Magn. Mater. **104–107**, 2059 (1992).
[9]S. Khmelevskyi and P. Mohn, Appl. Phys. Lett. **93**, 162503 (2008).
[10]M. Matsumoto, T. Kaneko, and K. Kamigaki, J. Phys. Soc. Jpn. **25**, 631 (1968).
[11]M. Matsumoto, S. Abe, H. Yoshida, S. Mori, T. Kanomata, and T. Kaneko, J. Magn. Magn. Mater. **104–107**, 2061 (1992).
[12]J. Wang, D. Wang, and Y. Kawazoe, Appl. Phys. Lett.**79**, 1507 (2001).
[13]Y. F. Xu, M. L. Yan, and D. J. Sellmyer, *Advanced Magnetic Nanostuctures*, edited by D. J. Sellmyer and R. Skomski (Springer, Berlin, 2006), p. 209.
[14]L. Zhang, D. Xue, and C. Gao, J. Magn. Magn. Mater. **267**, 111 (2003).
[15]H. Bi, S. Li, Y. Zhang, and Y. Du, J. Magn. Magn. Mater. **277**, 363 (2004).
[16]A. Mumtaz, K. Maaz, B. Janjua, S. K. Hasanain, and M. F. Bertino, J. Magn. Magn. Mater. **313**, 266 (2007).
[17]A. Punnoose, H. Magnone, and M. S. Seehra, Phys. Rev. B **64**, 174420 (2001).
[18]S. A. Makhlouf, F. T. Parker, F. E. Spada, and A. E. Berkowitz, J. Appl. Phys. **81**, 5561 (1997).
[19]L. Zhang, D. Xue, and C. Gao, J. Magn. Magn. Mater. **267**, 111 (2003).
[20]G. N. Rao, Y. D. Yao, and J. W. Chen, J. Appl. Phys. **105**, 093901 (2009).